



Variationally consistent multi-scale modeling and homogenization of stressed grain growth

Jiun-Shyan Chen ^{*}, Shafiqh Mehraeen

Department of Civil and Environmental Engineering, University of California, Los Angeles (UCLA), 5731G Boelter Hall, Los Angeles, CA 90095-1593, USA

Received 1 June 2003; received in revised form 26 October 2003; accepted 2 December 2003

Abstract

The macroscopic mechanical, thermal, and electromagnetic properties of materials are essentially determined by the microstructures of polycrystalline materials. This paper presents a multi-scale mathematical and computational framework for analyzing the global and local behavior of stressed grain growth. This is achieved by introducing an asymptotic expansion of field variables into the variational equation based on the principle of virtual power. The expanded variational equation gives rise to multi-scale Euler equations describing evolution processes at different scales, the scale-coupling relation, as well as the homogenized material properties. The multi-scale characteristics of grain boundary migration triggered by the multi-scale property of strain energy density jump across the grain boundaries are also discussed. A stressed grain growth example is analyzed to demonstrate multi-scale behavior of grain deformation and grain structure evolution under mechanical loading.

© 2004 Elsevier B.V. All rights reserved.

Keywords: Multi-scale; Asymptotic expansion; Grain growth; Grain boundary migration; Homogenization

1. Introduction

The microstructure of materials has been observed to have profound influence on a variety of properties of the material, such as the mechanical strength, toughness, electrical conductivity, magnetic susceptibility, etc. [5,10]. In recent years, various types of computer simulation methods have been developed for simulation of grain boundary migration.

The term “multi-scale analysis” has been used in the study of grain boundary migration, in which atomic-level simulation was employed to quantitatively capture the key grain boundary mechanisms and kinetics as the input for meso-scale grain boundary migration simulation [11]. For example, first principle calculations combined with a disclination-structural units model (DSUM) has been introduced for predicting grain boundary energies [21]. A work by coupling atomic simulation and finite element method [21]

^{*} Corresponding author.

E-mail address: jschen@seas.ucla.edu (J.-S. Chen).

has been presented for prediction of both short and long-period coincidence-site-lattice grain boundary energies. Molecular dynamic (MD) simulation has been used to determine the mechanism of grain growth in a nanocrystalline fcc metal [11]. It has been shown how first principle atomistics may be brought together with a continuum phase-field model, with the mixed-space cluster expansion (MSCE) serving as an intermediate tool to bridge from angstroms to microns [24]. In other applications where both atomic and continuum scales are to be resolved simultaneously, concurrent scale bridging becomes a critical issue to be addressed. Quasicontinuum method [12,22,23] has been proposed for problems requiring the simultaneous resolution of continuum and atomistic length scales in a unified manner. In this approach, the continuum part is furnished by finite element method where mesh adaptivity is employed to provide multi-scale analysis capabilities near lattice and other highly energetic regions, and proper weight distribution is introduced for handshaking regions. A bridging scale scheme has been proposed to separate basis functions of 2 scales in the handshaking region [26]. Based on the bridging scale technique and projection of the MD solution onto the coarse scale shape functions, a coupling of molecular dynamics and continuum mechanics simulations has been proposed [16,27]. In the context of multi-scale methods, a multi-resolution analysis by utilizing wavelet-like functions in the framework of meshfree method has also been introduced to construct hierarchical coarse–fine decomposition [14,15,30].

An effective multi-scale approach for solving problems with co-existing coarse and fine features is to construct a coarse scale problem that contains fine scale effects [8,9]. In [8,9], this is achieved by first decomposing coarse and fine scale problems, and expressing the fine scale solution in terms of the coarse solution. Then the fine scale solution is replaced by the coarse solution in the original problem, leading to a coarse scale problem that contains fine scale features. In one-dimension, an analytical relation between coarse and fine scale solutions can be derived [8]. In multi-dimensional case, certain assumptions were made to obtain the element level coarse–fine scale relation numerically [9]. These methods have been applied to the solution of strain localization problems. Analysis of heterogeneous materials represents another type of problems that exhibit multi-scale nature. Error estimate has been developed for identifying the error between the coarse scale solution using homogenized properties and the fine scale solution of the heterogeneous material with microstructures [18]. In the sub-domain with larger error, a local boundary value problem is solved, and this method was called the Homogenized Dirichlet Projection Method (HDPM). This approach was further extended to a hierarchical modeling of heterogeneous materials where the most essential scales of the problem can be adaptively selected in the discretization [19].

A systematic asymptotic expansion approach [1,3,20] for analyzing multiple physical processes interacting at multiple spatial scales has been introduced. In this approach, a series of rapidly varying spatial scales are introduced to capture the effects of spatial fluctuations induced by spatial heterogeneities. These spatial scales are introduced to the unknown variable through an asymptotic expansion. Consequently, the original differential equation can be separated into several leading order equations representing coarse and fine scale responses as well as scale-coupling relationship. The asymptotic expansion approach has been applied to homogenization of composites [6], multi-grid based method [7], and multi-physics problems with multiple spatial and temporal scales [29]. These works introduced asymptotic expansion directly to the differential equations (strong form) for scale decomposition.

The length scale of interest in this work is between an evolving meso-scale grain structure and a macro-scale continuum solid. In this paper, we introduce asymptotic expansion method to the variational equation of a stressed grain growth problem to obtain the multi-scale grain structure evolution equations as well as the homogenized material properties of a grain network. The content of this paper is organized as follows. The variational formulation for stressed grain growth based on principle of virtual power and the fundamental equations of asymptotic method are discussed in Section 2. Section 3 presents multi-scale decomposition of variational equations based on asymptotic expansion of field variables. The multi-scale Euler evolution equations for grain growth under the effect of external traction are presented in Section 4. In Section 5, discretization and numerical procedure are presented. In Section 6, a numerical example to

demonstrate the effectiveness of the proposed method and the multi-scale properties of the stressed grain growth processes are presented. Concluding remarks given in Section 7.

2. Basic equations

The multi-scale hierarchy from a macro-scale continuum to a meso-scale grain network of polycrystalline material under consideration is shown in Fig. 1.

Let \mathbf{x} -coordinate be the macro-scale coordinate system in the physical domain. A unit cell with domain Ω and boundary Γ of a continuum in the physical domain is mapped to referential domain Ω^y and boundary Γ^y measured by a meso-scale \mathbf{y} -coordinate. The macro- and meso-scale coordinates are related through a scaling parameter λ by

$$dy_i = \frac{dx_i}{\lambda}, \tag{2.1}$$

where λ is a very small real number. Thus a given length measured in the \mathbf{y} -coordinate is scaled by a factor $1/\lambda$ by its true scale measured in the \mathbf{x} -coordinate.

Consider a unit cell in the physical domain subjected to a surface traction \mathbf{h} on boundary Γ_h as shown in Fig. 2. The grain boundaries in the unit cell are denoted as Γ_{gb} . A variational equation for stressed grain growth based on the principle of virtual power described in the \mathbf{x} -coordinate [4] is as follows:

$$\delta\Pi(\mathbf{v}, \bar{\mathbf{v}}) = \delta\Pi_e(\mathbf{v}) + \delta\Pi_{gb}(\mathbf{v}, \bar{\mathbf{v}}) = 0, \tag{2.2}$$

$$\delta\Pi_e(\mathbf{v}) = \int_{\Omega} \frac{1}{2} \delta(\boldsymbol{\sigma} : \dot{\boldsymbol{\varepsilon}}) d\Omega - \int_{\Gamma_h} \delta\mathbf{v} \cdot \mathbf{h} d\Gamma - \int_{\Omega} \delta\mathbf{v} \cdot \mathbf{b} d\Omega, \tag{2.3}$$

$$\delta\Pi_{gb}(\mathbf{v}, \bar{\mathbf{v}}) = \int_{\Gamma_{gb}} \frac{1}{2} (\boldsymbol{\sigma}^+ : \boldsymbol{\varepsilon}^+ - \boldsymbol{\sigma}^- : \boldsymbol{\varepsilon}^-) \delta\bar{v}_n d\Gamma + \int_{\Gamma_{gb}} \gamma \left(\frac{\partial \delta\bar{v}_s}{\partial s} + \frac{\delta\bar{v}_n}{R} \right) d\Gamma + \int_{\Gamma_{gb}} \frac{\delta\bar{v}_n}{\mu} \bar{v}_n d\Gamma, \tag{2.4}$$

where $\delta\Pi_e$ is the virtual power associated with grain deformation, $\delta\Pi_{gb}$ is the virtual power associated with driving forces acting on grain boundaries, \mathbf{v} is the grain material velocity, $\bar{\mathbf{v}}$ is the grain boundary migration velocity, \bar{v}_n is the normal velocity pointing away from the center of curvature of the grain boundary, \bar{v}_s is the tangential velocity along the grain boundary, s is the coordinate along the grain boundary, γ is the surface tension (the boundary energy per unit area), R is the radius of curvature of the grain boundary, μ is the mobility representing the ease with which the grain boundary can migrate, \mathbf{h} is the surface traction applied

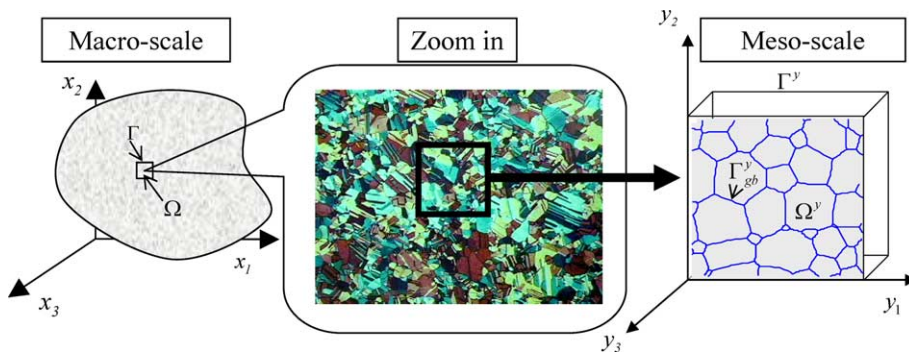


Fig. 1. Length scale hierarchy of continuum and grain network.

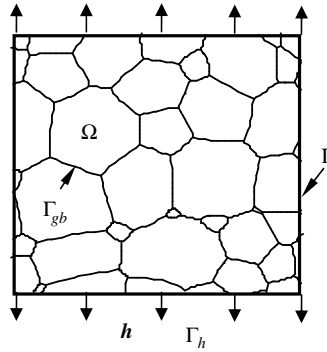


Fig. 2. Unit cell structure of stressed grain network.

on the traction boundary Γ_h , \mathbf{b} is body force, σ^+ , ϵ^+ are the stress and strain in the grain that gains virtual area $\delta\bar{v}_n d\Gamma$ (grain A), respectively, and σ^- , ϵ^- are the stress and strain in the grain located on the other side of the boundary (grain B), respectively, as shown in Fig. 3. The detail discussions can be found in [4]. We assume the stress-strain relation follows an anisotropic creep law:

$$\sigma_{ij} = C_{ijkl} \dot{\epsilon}_{kl}. \tag{2.5}$$

To describe the multi-scale material behavior, the material velocity \mathbf{v} is expressed in the following asymptotic expansion form

$$v_i(\mathbf{x}, \mathbf{y}) = v_i^{[0]}(\mathbf{x}, \mathbf{y}) + \lambda v_i^{[1]}(\mathbf{x}, \mathbf{y}) + O(\lambda^2), \tag{2.6}$$

where $v_i^{[0]}$ and $v_i^{[1]}$ are macro (coarse)-scale and meso (fine)-scale components of material velocity, respectively, and the superscript $[n]$ denotes the level of scale.

For a function expressed in both coarse and fine scale coordinates, the following relationship can be obtained,

$$\frac{\partial}{\partial x_i} = \frac{\partial}{\partial x_i} \Big|_{[y]} + \frac{\partial}{\partial y_i} \Big|_{[x]} \frac{\partial y_i}{\partial x_i} = \frac{\partial}{\partial x_i} \Big|_{[y]} + \frac{1}{\lambda} \frac{\partial}{\partial y_i} \Big|_{[x]}. \tag{2.7}$$

In the following derivation, we drop the subscripts $[x]$ and $[y]$ for notational simplicity. Using Eq. (2.7), strain rate $\dot{\epsilon}_{ij}$ is expressed as

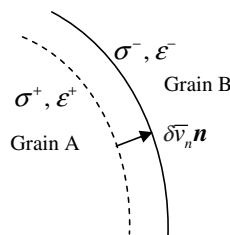


Fig. 3. Strain energy change due to grain boundary migration.

$$\begin{aligned} \dot{\epsilon}_{ij} = & \frac{1}{2} \left(\frac{\partial v_i^{[0]}}{\partial x_j} + \frac{\partial v_j^{[0]}}{\partial x_i} \right) + \frac{1}{2\lambda} \left(\frac{\partial v_i^{[0]}}{\partial y_j} + \frac{\partial v_j^{[0]}}{\partial y_i} \right) + \frac{\lambda}{2} \left(\frac{\partial v_i^{[1]}}{\partial x_j} + \frac{\partial v_j^{[1]}}{\partial x_i} \right) + \frac{1}{2} \left(\frac{\partial v_i^{[1]}}{\partial y_j} + \frac{\partial v_j^{[1]}}{\partial y_i} \right) \\ & + \frac{\lambda^2}{2} \left(\frac{\partial v_i^{[2]}}{\partial x_j} + \frac{\partial v_j^{[2]}}{\partial x_i} \right) + \frac{\lambda}{2} \left(\frac{\partial v_i^{[2]}}{\partial y_j} + \frac{\partial v_j^{[2]}}{\partial y_i} \right) + \dots \end{aligned} \tag{2.8}$$

We further define the following notations

$$\begin{aligned} \dot{\epsilon}_{ij}^{[k]} &= \frac{1}{2} \left(\frac{\partial v_i^{[k]}}{\partial x_j} + \frac{\partial v_j^{[k]}}{\partial x_i} \right), \\ \dot{\epsilon}_{ij}^{[k]} &= \frac{1}{2} \left(\frac{\partial v_i^{[k]}}{\partial y_j} + \frac{\partial v_j^{[k]}}{\partial y_i} \right) \end{aligned} \tag{2.9}$$

and re-express the strain rate expansion as

$$\begin{aligned} \dot{\epsilon}_{ij} = & \lambda^{-1} \dot{\epsilon}_{ij}^{[0]} + \left(\dot{\epsilon}_{ij}^{[0]} + \dot{\epsilon}_{ij}^{[1]} \right) + \lambda \left(\dot{\epsilon}_{ij}^{[1]} + \dot{\epsilon}_{ij}^{[2]} \right) + \lambda^2 \left(\dot{\epsilon}_{ij}^{[2]} + \dot{\epsilon}_{ij}^{[3]} \right) + \dots \\ = & \lambda^{-1} \dot{\epsilon}_{ij}^{[-1]} + \dot{\epsilon}_{ij}^{[0]} + \lambda^1 \dot{\epsilon}_{ij}^{[1]} + \lambda^2 \dot{\epsilon}_{ij}^{[2]} + \dots, \end{aligned} \tag{2.10}$$

where for convenience we have introduced the following notations:

$$\dot{\epsilon}_{ij}^{[-1]} = \dot{\epsilon}_{ij}^{[0]} = \frac{1}{2} \left(\frac{\partial v_i^{[0]}}{\partial y_j} + \frac{\partial v_j^{[0]}}{\partial y_i} \right), \tag{2.11}$$

$$\dot{\epsilon}_{ij}^{[k]} = \left(\dot{\epsilon}_{ij}^{[k]} + \dot{\epsilon}_{ij}^{[k+1]} \right), \quad \forall k \geq 0, k \in \mathbb{Z}. \tag{2.12}$$

For a creep law with stress–strain relation in Eq. (2.5), the expansion of stress field is obtained as

$$\sigma_{ij} = \lambda^{-1} \sigma_{ij}^{[-1]} + \sigma_{ij}^{[0]} + \lambda \sigma_{ij}^{[1]} + \lambda^2 \sigma_{ij}^{[2]} + \dots, \tag{2.13}$$

where

$$\sigma_{ij}^{[k]} = C_{ijkl} \dot{\epsilon}_{kl}^{[k]}. \tag{2.14}$$

3. Multi-scale variational formulation

The hierarchical decomposition of the variational formulation into its coarse and fine scale components is obtained by introducing asymptotic expansions of material velocities, strain rates, and stress into Eq. (2.2). First, consider multi-scale expression of strain energy density rate in $\delta \Pi_e$ of Eq. (2.3) as follows:

$$\begin{aligned} \int_{\Omega} \frac{1}{2} \delta(\dot{\epsilon} : \sigma) \, d\Omega = & \lambda^{-2} \int_{\Omega} \frac{1}{2} \delta \left(\dot{\epsilon}_{ij}^{[-1]} \sigma_{ij}^{[-1]} \right) \, d\Omega + \lambda^{-1} \int_{\Omega} \frac{1}{2} \delta \left(\dot{\epsilon}_{ij}^{[-1]} \sigma_{ij}^{[0]} + \dot{\epsilon}_{ij}^{[0]} \sigma_{ij}^{[-1]} \right) \, d\Omega \\ & + \int_{\Omega} \frac{1}{2} \delta \left(\dot{\epsilon}_{ij}^{[-1]} \sigma_{ij}^{[1]} + \dot{\epsilon}_{ij}^{[0]} \sigma_{ij}^{[0]} + \dot{\epsilon}_{ij}^{[1]} \sigma_{ij}^{[-1]} \right) \, d\Omega + \lambda^1 \int_{\Omega} \frac{1}{2} \delta \left(\dot{\epsilon}_{ij}^{[1]} \sigma_{ij}^{[0]} + \dot{\epsilon}_{ij}^{[0]} \sigma_{ij}^{[1]} \right) \, d\Omega + \mathcal{O}(\lambda^2). \end{aligned} \tag{3.1}$$

Similarly, the surface traction and body force terms of $\delta \Pi_e$ are expanded as

$$\int_{\Gamma_h} \delta \mathbf{v} \cdot \mathbf{h} \, d\Gamma = \int_{\Gamma_h} \delta v_i^{[0]} h_i \, d\Gamma + \lambda \int_{\Gamma_h} \delta v_i^{[1]} h_i \, d\Gamma + \mathcal{O}(\lambda^2) \tag{3.2}$$

and

$$\int_{\Omega} \delta \mathbf{v} \cdot \mathbf{b} \, d\Gamma = \int_{\Omega} \delta v_i^{[0]} b_i \, d\Gamma + \lambda \int_{\Omega} \delta v_i^{[1]} b_i \, d\Gamma + \mathcal{O}(\lambda^2). \quad (3.3)$$

Thus we have

$$\begin{aligned} \delta \Pi_e(\mathbf{v}^{[0]} + \lambda \mathbf{v}^{[1]}) &= \lambda^{-2} \left(\int_{\Omega} \frac{1}{2} \delta \left(\dot{\epsilon}_{ij}^{[-1]} \sigma_{ij}^{[-1]} \right) \, d\Omega \right) + \lambda^{-1} \left(\int_{\Omega} \frac{1}{2} \delta \left(\dot{\epsilon}_{ij}^{[-1]} \sigma_{ij}^{[0]} + \dot{\epsilon}_{ij}^{[0]} \sigma_{ij}^{[-1]} \right) \, d\Omega \right) \\ &\quad + \left(\int_{\Omega} \frac{1}{2} \delta \left(\dot{\epsilon}_{ij}^{[-1]} \sigma_{ij}^{[1]} + \dot{\epsilon}_{ij}^{[0]} \sigma_{ij}^{[0]} + \dot{\epsilon}_{ij}^{[1]} \sigma_{ij}^{[-1]} \right) \, d\Omega - \int_{\Gamma_h} \delta \mathbf{v}^{[0]} \cdot \mathbf{h} \, d\Gamma - \int_{\Omega} \delta \mathbf{v}^{[0]} \cdot \mathbf{b} \, d\Omega \right) + \mathcal{O}(\lambda). \end{aligned} \quad (3.4)$$

The total virtual power takes the following decomposed form

$$\delta \Pi(\mathbf{v}^{[0]} + \lambda \mathbf{v}^{[1]}, \bar{\mathbf{v}}) = \lambda^{-2} \delta \Pi^{[-2]} + \lambda^{-1} \delta \Pi^{[-1]} + \delta \Pi^{[0]} + \mathcal{O}(\lambda) = 0, \quad (3.5)$$

where

$$\delta \Pi^{[-2]} = \delta \Pi_e^{[-2]}(\mathbf{v}) = \int_{\Omega} \frac{1}{2} \delta \left(\dot{\epsilon}_{ij}^{[-1]} \sigma_{ij}^{[-1]} \right) \, d\Omega, \quad (3.6)$$

$$\delta \Pi^{[-1]} = \delta \Pi_e^{[-1]}(\mathbf{v}) = \int_{\Omega} \frac{1}{2} \delta \left(\dot{\epsilon}_{ij}^{[-1]} \sigma_{ij}^{[0]} + \dot{\epsilon}_{ij}^{[0]} \sigma_{ij}^{[-1]} \right) \, d\Omega, \quad (3.7)$$

$$\delta \Pi^{[0]} = \delta \Pi^{[0]}(\mathbf{v}, \bar{\mathbf{v}}) = \delta \Pi_e^{[0]}(\mathbf{v}) + \delta \Pi_{\text{gb}}(\mathbf{v}, \bar{\mathbf{v}}), \quad (3.8)$$

$$\delta \Pi_e^{[0]}(\mathbf{v}) = \int_{\Omega} \frac{1}{2} \delta \left(\dot{\epsilon}_{ij}^{[-1]} \sigma_{ij}^{[1]} + \dot{\epsilon}_{ij}^{[0]} \sigma_{ij}^{[0]} + \dot{\epsilon}_{ij}^{[1]} \sigma_{ij}^{[-1]} \right) \, d\Omega - \int_{\Gamma_h} \delta v_i^{[0]} h_i \, d\Gamma - \int_{\Omega} \delta v_i^{[0]} b_i \, d\Omega, \quad (3.9)$$

Eq. (3.5) leads to $\delta \Pi^{[-2]} = \delta \Pi^{[-1]} = \delta \Pi^{[0]} = 0$ when $\lambda \rightarrow 0$. Further, since the terms $\delta \Pi_e^{[0]}(\mathbf{v})$ and $\delta \Pi_{\text{gb}}(\mathbf{v}, \bar{\mathbf{v}})$ are associated with virtual material and grain boundary velocities, respectively, $\delta \Pi^{[0]}(\mathbf{v}) = 0$ renders $\delta \Pi_e^{[0]}(\mathbf{v}) = 0$ and $\delta \Pi_{\text{gb}}(\mathbf{v}, \bar{\mathbf{v}}) = 0$. In summary, we have

$$I_1 = \delta \Pi_e^{[-2]}(\mathbf{v}) = \int_{\Omega} \frac{1}{2} \delta \left(\dot{\epsilon}_{ij}^{[-1]} \sigma_{ij}^{[-1]} \right) \, d\Omega = 0, \quad (3.10)$$

$$I_2 = \delta \Pi_e^{[-1]}(\mathbf{v}) = \int_{\Omega} \frac{1}{2} \delta \left(\dot{\epsilon}_{ij}^{[-1]} \sigma_{ij}^{[0]} + \dot{\epsilon}_{ij}^{[0]} \sigma_{ij}^{[-1]} \right) \, d\Omega = 0, \quad (3.11)$$

$$I_3 = \delta \Pi_e^{[0]}(\mathbf{v}) = \int_{\Omega} \frac{1}{2} \delta \left(\dot{\epsilon}_{ij}^{[-1]} \sigma_{ij}^{[1]} + \dot{\epsilon}_{ij}^{[0]} \sigma_{ij}^{[0]} + \dot{\epsilon}_{ij}^{[1]} \sigma_{ij}^{[-1]} \right) \, d\Omega - \int_{\Gamma_h} \delta \mathbf{v}^{[0]} \cdot \mathbf{h} \, d\Gamma - \int_{\Omega} \delta \mathbf{v}^{[0]} \cdot \mathbf{b} \, d\Omega = 0, \quad (3.12)$$

$$I_4 = \delta \Pi_{\text{gb}}(\mathbf{v}, \bar{\mathbf{v}}) = \int_{\Gamma_{\text{gb}}} \frac{1}{2} (\sigma_{ij}^+ \epsilon_{ij}^+ - \sigma_{ij}^- \epsilon_{ij}^-) \delta \bar{v}_n \, d\Gamma + \int_{\Gamma_{\text{gb}}} \gamma \left(\frac{\partial \delta \bar{v}_s}{\partial s} + \frac{\delta \bar{v}_n}{R} \right) \, d\Gamma + \int_{\Gamma_{\text{gb}}} \frac{\delta \bar{v}_n}{\mu} \bar{v}_n \, d\Gamma = 0. \quad (3.13)$$

4. Multi-scale evolution equations

In this section, the governing equations for different scales will be obtained using the decomposed variational formulation discussed in Section 3.

4.1. Coarse scale property of material velocity ($I_1 = 0$)

The first leading order equation (3.6) gives

$$I_1 = \int_{\Omega} \frac{1}{2} \delta \left(\dot{\hat{\epsilon}}_{ij}^{[-1]} \sigma_{ij}^{[-1]} \right) d\Omega = \frac{1}{4} \int_{\Omega} \left(\frac{\partial \delta v_i^{[0]}}{\partial y_j} + \frac{\partial \delta v_j^{[0]}}{\partial y_i} \right) C_{ijkl} \dot{\hat{\epsilon}}_{kl}^{[-1]} d\Omega, \tag{4.1}$$

where C_{ijkl} is assumed to have minor symmetry. Further consider domain mapping, Eq. (4.1) can be expressed as

$$\begin{aligned} I_1 &= \frac{1}{4} \int_{\Omega^v} \lambda^2 \left(\frac{\partial \delta v_i^{[0]}}{\partial y_j} + \frac{\partial \delta v_j^{[0]}}{\partial y_i} \right) \sigma_{ij}^{[-1]} d\Omega \\ &= \frac{1}{4} \left\{ \lambda \int_{\Gamma} \sigma_{ij}^{[-1]} \left(\delta v_i^{[0]} n_j + \delta v_j^{[0]} n_i \right) d\Gamma - \int_{\Omega} \frac{\partial \sigma_{ij}^{[-1]}}{\partial y_j} \delta v_i^{[0]} d\Omega - \int_{\Omega} \frac{\partial \sigma_{ij}^{[-1]}}{\partial y_i} \delta v_j^{[0]} d\Omega \right\} \\ &= -\frac{1}{4} \int_{\Omega} \left(\frac{\partial \sigma_{ij}^{[-1]}}{\partial y_i} \delta v_j^{[0]} + \frac{\partial \sigma_{ij}^{[-1]}}{\partial y_j} \delta v_i^{[0]} \right) d\Omega. \end{aligned} \tag{4.2}$$

Here we have used the property that the boundary term vanishes as λ approaches zero. Further considering symmetric stress tensor, one has

$$I_1 = -\frac{1}{2} \int_{\Omega} \frac{\partial \sigma_{ij}^{[-1]}}{\partial y_i} \delta v_j^{[0]} d\Omega = 0. \tag{4.3}$$

Due to the arbitrariness of $\delta v_j^{[0]}$ in Ω , Eq. (4.3) yields

$$\frac{\partial \sigma_{ij}^{[-1]}}{\partial y_i} = 0 \quad \text{in } \Omega. \tag{4.4}$$

Consequently,

$$\frac{\partial}{\partial y_j} \left(C_{ijke} \dot{\hat{\epsilon}}_{ke}^{[-1]} \right) = \frac{1}{2} \frac{\partial}{\partial y_j} \left(C_{ijke} \left(\frac{\partial v_k^{[0]}}{\partial y_e} + \frac{\partial v_e^{[0]}}{\partial y_k} \right) \right) = 0. \tag{4.5}$$

Recasting Eq. (4.5) in the weak form in reference domain Ω^v and using integration by parts gives rise to

$$\begin{aligned} \int_{\Omega^v} v_i^{[0]} \frac{1}{2} \frac{\partial}{\partial y_j} \left(C_{ijke} \left(\frac{\partial v_k^{[0]}}{\partial y_e} + \frac{\partial v_e^{[0]}}{\partial y_k} \right) \right) d\Omega &= - \int_{\Omega^v} \frac{\partial v_i^{[0]}}{\partial y_j} \frac{1}{2} \left(C_{ijke} \left(\frac{\partial v_k^{[0]}}{\partial y_e} + \frac{\partial v_e^{[0]}}{\partial y_k} \right) \right) d\Omega \\ &\quad + \int_{\Gamma^v} v_i^{[0]} \left(C_{ijke} \dot{\hat{\epsilon}}_{ke}^{[-1]} n_j \right) d\Gamma = 0. \end{aligned} \tag{4.6}$$

By employing periodicity of the unit cell in Ω^v , the last integral vanishes. Since C_{ijke} is assumed to be positive definite, we have

$$\frac{\partial v_i^{[0]}}{\partial y_j} = 0 \quad \therefore \quad v_i^{[0]} = v_i^{[0]}(\mathbf{x}). \tag{4.7}$$

Hence the coarse scale component of the solution $v_i^{[0]}$ is only function of \mathbf{x} . This yields

$$\dot{\hat{\epsilon}}_{ij}^{[-1]} \equiv \dot{\hat{\epsilon}}_{ij}^{[0]} = \frac{1}{2} \left(\frac{\partial v_i^{[0]}}{\partial y_j} + \frac{\partial v_j^{[0]}}{\partial y_i} \right) = 0, \quad \sigma_{ij}^{[-1]} = C_{ijkl} \dot{\hat{\epsilon}}_{kl}^{[-1]} = 0. \tag{4.8}$$

4.2. Scale coupling in material velocity ($I_2 = 0$)

Similarly, for the next leading order term $I_2 = 0$, we have

$$I_2 = \int_{\Omega} \frac{1}{2} \delta \left(\dot{\epsilon}_{ij}^{[-1]} \sigma_{ij}^{[0]} + \dot{\epsilon}_{ij}^{[0]} \sigma_{ij}^{[-1]} \right) d\Omega = \int_{\Omega} \delta \left(\dot{\epsilon}_{ij}^{[0]} C_{ijkl} \left(\dot{\epsilon}_{kl}^{[0]} + \dot{\epsilon}_{kl}^{[1]} \right) \right) d\Omega. \quad (4.9)$$

By the major symmetry of C_{ijkl} , Eq. (4.9) can be rewritten as

$$\begin{aligned} I_2 &= \int_{\Omega} \left(\delta \dot{\epsilon}_{ij}^{[0]} \sigma_{ij}^{[0]} + \dot{\epsilon}_{ij}^{[0]} C_{ijkl} \left(\delta \dot{\epsilon}_{kl}^{[0]} + \delta \dot{\epsilon}_{kl}^{[1]} \right) \right) d\Omega = \int_{\Omega} \left(\delta \dot{\epsilon}_{ij}^{[0]} \sigma_{ij}^{[0]} + \left(\delta \dot{\epsilon}_{kl}^{[0]} + \delta \dot{\epsilon}_{kl}^{[1]} \right) \sigma_{kl}^{[-1]} \right) d\Omega \\ &= \frac{1}{2} \int_{\Omega} \left(\left(\frac{\partial \delta v_i^{[0]}}{\partial y_j} + \frac{\partial \delta v_j^{[0]}}{\partial y_i} \right) \sigma_{ij}^{[0]} + \left(\left(\frac{\partial \delta v_i^{[0]}}{\partial x_j} + \frac{\partial \delta v_j^{[0]}}{\partial x_i} \right) + \left(\frac{\partial \delta v_i^{[1]}}{\partial y_j} + \frac{\partial \delta v_j^{[1]}}{\partial y_i} \right) \right) \sigma_{ij}^{[-1]} \right) d\Omega. \end{aligned} \quad (4.10)$$

Further considering symmetry of $\sigma_{ij}^{[k]}$, and small parameter $\lambda \rightarrow 0$, we have

$$\begin{aligned} I_2 &= \int_{\Omega} \frac{\partial \delta v_i^{[0]}}{\partial y_j} \sigma_{ij}^{[0]} d\Omega + \int_{\Omega} \left(\frac{\partial \delta v_i^{[0]}}{\partial x_j} + \frac{\partial \delta v_i^{[1]}}{\partial y_j} \right) \sigma_{ij}^{[-1]} d\Omega \\ &= \lambda \left(\int_{\Gamma} \delta v_i^{[0]} \sigma_{ij}^{[0]} n_j d\Gamma + \int_{\Gamma} \delta v_i^{[1]} \sigma_{ij}^{[-1]} n_j d\Gamma \right) + \int_{\Gamma} \delta v_i^{[0]} \sigma_{ij}^{[-1]} n_j d\Gamma \\ &\quad - \int_{\Omega} \frac{\partial \sigma_{ij}^{[0]}}{\partial y_j} \delta v_i^{[0]} d\Omega - \int_{\Omega} \frac{\partial \sigma_{ij}^{[-1]}}{\partial x_j} \delta v_i^{[0]} d\Omega - \int_{\Omega} \frac{\partial \sigma_{ij}^{[-1]}}{\partial y_j} \delta v_i^{[1]} d\Omega \\ &= - \int_{\Omega} \left(\frac{\partial \sigma_{ij}^{[0]}}{\partial y_j} + \frac{\partial \sigma_{ij}^{[-1]}}{\partial x_j} \right) \delta v_i^{[0]} d\Omega - \int_{\Omega} \frac{\partial \sigma_{ij}^{[-1]}}{\partial y_j} \delta v_i^{[1]} d\Omega. \end{aligned} \quad (4.11)$$

Substitution of Eq. (4.4) into Eq. (4.11) yields

$$I_2 = - \int_{\Omega} \left(\frac{\partial \sigma_{ij}^{[0]}}{\partial y_j} + \frac{\partial \sigma_{ij}^{[-1]}}{\partial x_j} \right) \delta v_i^{[0]} d\Omega = 0. \quad (4.12)$$

The arbitrariness of $\delta v_i^{[0]}$ in Ω yields

$$\frac{\partial \sigma_{ij}^{[0]}}{\partial y_j} + \frac{\partial \sigma_{ij}^{[-1]}}{\partial x_j} = 0 \quad \text{in } \Omega. \quad (4.13)$$

Further using results in Eq. (4.8), Eq. (4.13) leads to

$$\frac{\partial \sigma_{ij}^{[0]}}{\partial y_j} = 0 \quad (4.14)$$

or

$$\frac{\partial}{\partial y_j} \left[C_{ijkl} \left(\dot{\epsilon}_{kl}^{[0]} + \dot{\epsilon}_{kl}^{[1]} \right) \right] = 0. \quad (4.15)$$

It can be shown [3] that for Eq. (4.15) to hold, the coarse and fine scale material velocities should have the following relation

$$v_k^{[1]} = \alpha_{kmn}(y) \dot{\epsilon}_{mn}^{[0]}(x). \tag{4.16}$$

The strain rate can be rewritten as

$$\dot{\epsilon}_{ij}^{[1]} = \frac{1}{2} \left(\frac{\partial v_i^{[1]}}{\partial y_j} + \frac{\partial v_j^{[1]}}{\partial y_i} \right) = \dot{\epsilon}_{mn}^{[0]} \eta_{ijmn}, \tag{4.17}$$

where

$$\eta_{ijmn} = \frac{1}{2} \left(\frac{\partial \alpha_{imn}}{\partial y_j} + \frac{\partial \alpha_{jmn}}{\partial y_i} \right). \tag{4.18}$$

Substitution of Eq. (4.17) into Eq. (4.15) gives

$$\frac{\partial}{\partial y_j} \left[C_{ijkl} \left(\dot{\epsilon}_{kl}^{[0]} + \dot{\epsilon}_{mn}^{[0]} \eta_{klmn} \right) \right] = \dot{\epsilon}_{mn}^{[0]} \frac{\partial}{\partial y_j} [C_{ijkl} (I_{klmn} + \eta_{klmn})] = 0, \quad \forall \dot{\epsilon}_{mn}^{[0]}, \tag{4.19}$$

where

$$I_{klmn} = \frac{1}{2} (\delta_{km} \delta_{ln} + \delta_{kn} \delta_{lm}). \tag{4.20}$$

Eq. (4.19) leads to

$$\frac{\partial}{\partial y_j} [C_{ijkl} (I_{klmn} + \eta_{klmn})] = 0. \tag{4.21}$$

The coupling function $\alpha_{kmn}(y)$ involved in Eq. (4.21) can be obtained by a Galerkin approximation of the following weak form:

$$\int_{\Omega^v} \beta_{imn} \frac{\partial}{\partial y_j} [C_{ijkl} (I_{klmn} + \eta_{klmn})] \, d\Omega = 0, \tag{4.22}$$

where β_{imn} is a weight function. By integration by parts and periodicity, Eq. (4.22) can be expressed as

$$\int_{\Omega^v} \beta_{imn,j} C_{ijkl} \eta_{klmn} \, d\Omega = - \int_{\Omega^v} \beta_{imn,j} C_{ijmn} \, d\Omega. \tag{4.23}$$

4.3. Coarse and fine scales of grain deformation ($I_3 = 0$)

Once the coupling function $\alpha_{kmn}(y)$ is solved from Eq. (4.23), the coarse scale and fine scale components of material velocity can be obtained by using the equation $I_3 = 0$ as follows

$$\begin{aligned} I_3 &= \delta \Pi_e^{[0]} = \int_{\Omega} \frac{1}{2} \delta \left(\dot{\epsilon}_{ij}^{[-1]} \sigma_{ij}^{[1]} + \dot{\epsilon}_{ij}^{[0]} \sigma_{ij}^{[0]} + \dot{\epsilon}_{ij}^{[1]} \sigma_{ij}^{[-1]} \right) \, d\Omega - \int_{\Gamma} \delta v_i^{[0]} h_i \, d\Gamma - \int_{\Omega} \delta v_i^{[0]} b_i \, d\Omega \\ &= \frac{1}{2} \int_{\Omega} \delta \left(2 \dot{\epsilon}_{ij}^{[0]} C_{ijkl} \left(\dot{\epsilon}_{kl}^{[1]} + \dot{\epsilon}_{kl}^{[2]} \right) + \left(\dot{\epsilon}_{ij}^{[0]} + \dot{\epsilon}_{ij}^{[1]} \right) C_{ijkl} \left(\dot{\epsilon}_{kl}^{[0]} + \dot{\epsilon}_{kl}^{[1]} \right) \right) \, d\Omega \\ &\quad - \int_{\Gamma} \delta v_i^{[0]} h_i \, d\Gamma - \int_{\Omega} \delta v_i^{[0]} b_i \, d\Omega = 0. \end{aligned} \tag{4.24}$$

Using symmetric properties of C_{ijkl} , we arrive the following equation:

$$\begin{aligned}
 I_3 &= \lambda \int_{\Gamma} \delta v_i^{[0]} \sigma_{ij}^{[1]} n_j d\Gamma - \int_{\Omega} \delta v_i^{[0]} \frac{\partial \sigma_{ij}^{[1]}}{\partial y_j} d\Omega + \int_{\Gamma} \delta v_i^{[1]} \sigma_{ij}^{[-1]} n_j d\Gamma - \int_{\Omega} \delta v_i^{[1]} \frac{\partial \sigma_{ij}^{[-1]}}{\partial y_j} d\Omega \\
 &+ \lambda \int_{\Gamma} \delta v_i^{[2]} \sigma_{ij}^{[-1]} n_j d\Gamma - \int_{\Omega} \delta v_i^{[2]} \frac{\partial \sigma_{ij}^{[-1]}}{\partial y_j} d\Omega + \int_{\Gamma} \delta v_i^{[0]} \sigma_{ij}^{[0]} n_j d\Gamma - \int_{\Omega} \delta v_i^{[0]} \frac{\partial \sigma_{ij}^{[0]}}{\partial y_j} d\Omega \\
 &+ \lambda \int_{\Gamma} \delta v_i^{[1]} \sigma_{ij}^{[0]} n_j d\Gamma - \int_{\Omega} \delta v_i^{[1]} \frac{\partial \sigma_{ij}^{[0]}}{\partial y_j} d\Omega - \int_{\Gamma_h} \delta v_i^{[0]} h_i d\Gamma - \int_{\Omega} \delta v_i^{[0]} b_i d\Omega \\
 &= - \int_{\Omega} \left(\frac{\partial \sigma_{ij}^{[1]}}{\partial y_j} + \frac{\partial \sigma_{ij}^{[0]}}{\partial x_j} \right) \delta v_i^{[0]} d\Omega - \int_{\Omega} \left(\frac{\partial \sigma_{ij}^{[-1]}}{\partial x_j} + \frac{\partial \sigma_{ij}^{[0]}}{\partial y_j} \right) \delta v_i^{[1]} d\Omega - \int_{\Omega} \frac{\partial \sigma_{ij}^{[-1]}}{\partial y_j} \delta v_i^{[2]} d\Omega \\
 &+ \int_{\Gamma} \delta v_i^{[0]} \sigma_{ij}^{[0]} n_j d\Gamma + \int_{\Gamma} \delta v_i^{[1]} \sigma_{ij}^{[-1]} n_j d\Gamma - \int_{\Gamma_h} \delta v_i^{[0]} h_i d\Gamma - \int_{\Omega} \delta v_i^{[0]} b_i d\Omega = 0. \tag{4.25}
 \end{aligned}$$

Further considering Eqs. (4.8) and (4.13), Eq. (4.25) can be reduced to

$$I_3 = - \int_{\Omega} \left(\frac{\partial \sigma_{ij}^{[1]}}{\partial y_j} + \frac{\partial \sigma_{ij}^{[0]}}{\partial x_j} + b_i \right) \delta v_i^{[0]} d\Omega + \int_{\Gamma_h} \delta v_i^{[0]} (\sigma_{ij}^{[0]} n_j - h_i) d\Gamma = 0. \tag{4.26}$$

This gives rise to the following equilibrium equation of the coarse scale problem and corresponding natural boundary conditions

$$\frac{\partial \sigma_{ij}^{[1]}}{\partial y_j} + \frac{\partial \sigma_{ij}^{[0]}}{\partial x_j} + b_i = 0 \quad \text{on } \Omega, \tag{4.27}$$

$$\sigma_{ij}^{[0]} n_j - h_i = 0, \quad \text{on } \Gamma_h. \tag{4.28}$$

By integrating both sides of Eq. (4.27) over the referential unit cell Ω^y and employing the periodicity of the unit cell, we have

$$\int_{\Omega^y} \left(\frac{\partial \sigma_{ij}^{[0]}}{\partial x_j} + \frac{\partial \sigma_{ij}^{[1]}}{\partial y_j} + b_i \right) d\Omega = \int_{\Omega^y} \frac{\partial \sigma_{ij}^{[0]}}{\partial x_j} d\Omega + \int_{\Gamma_h^y} \sigma_{ij}^{[1]} n_j d\Gamma + S b_i = 0, \tag{4.29}$$

where S is the area of the unit cell. Note that second integral on R.H.S. of Eq. (4.29) drops due to periodic boundary conditions. Further introducing the coupling relation between coarse and fine scales in (4.17), Eq. (4.29) can be recast to result in the following macroscopic problem

$$\bar{C}_{ijkl} \frac{\partial \dot{\varepsilon}_{kl}^{[0]}}{\partial x_j} + b_i = 0 \quad \text{in } \Omega^y, \tag{4.30}$$

$$\sigma_{ij}^{[0]} n_j - h_i = 0 \quad \text{on } \Gamma_h^y, \tag{4.31}$$

where

$$\bar{C}_{ijmn} = \frac{1}{S} \int_{\Omega^y} C_{ijkl} (I_{klmn} + \eta_{klmn}) d\Omega. \tag{4.32}$$

The term \bar{C}_{ijkl} represents the homogenized constitutive tensor of C_{ijkl} based on grain structure. The weak form of problem (4.30) and (4.31) reads

$$\int_{\Omega^y} \frac{\partial w_i}{\partial x_j} \bar{C}_{ijkl} \dot{\epsilon}_{kl}^{[0]} d\Omega - \int_{\Gamma_h^y} w_i h_i d\Gamma - \int_{\Omega^y} w_i b_i d\Omega = 0, \tag{4.33}$$

where w_i is the weight function.

4.4. Multi-scale grain boundary evolution ($I_4 = 0$)

Finally the grain boundary evolution equation is obtained using $I_4 = 0$ in Eq. (3.13). The grain boundary velocity $\bar{\mathbf{v}}$ in response to the coarse and fine scale driving forces associated with the strain energy density jump $(\boldsymbol{\sigma}^+ : \boldsymbol{\varepsilon}^+ - \boldsymbol{\sigma}^- : \boldsymbol{\varepsilon}^-)/2$ across the grain boundary can be expressed as

$$\bar{v}_i(\mathbf{x}, \mathbf{y}) = \bar{v}_i^{[0]}(\mathbf{x}, \mathbf{y}) + \lambda \bar{v}_i^{[1]}(\mathbf{x}, \mathbf{y}) + O(\lambda^2), \tag{4.34}$$

where $\bar{v}_i^{[0]}$ and $\bar{v}_i^{[1]}$ are the components of \bar{v}_i dictated by the coarse and fine scale components of the driving force motivated by the strain energy density jump. Substituting expansion equations (4.34), (2.6), and the expanded strain rate and stress in (2.10) and (2.13), into (3.13), together with the coarse scale relation (4.8), we obtain the following decomposed grain boundary evolution equation

$$\begin{aligned} \delta \Pi_{\text{gb}}(\mathbf{v}, \bar{\mathbf{v}}) &= \int_{\Gamma_{\text{gb}}^y} \frac{1}{2} \left(\left[\varepsilon_{ij}^{+[0]} \sigma_{ij}^{+[0]} - \varepsilon_{ij}^{-[0]} \sigma_{ij}^{-[0]} \right] + \lambda \left[\varepsilon_{ij}^{+[0]} \sigma_{ij}^{+[1]} + \varepsilon_{ij}^{+[1]} \sigma_{ij}^{+[0]} - \varepsilon_{ij}^{-[0]} \sigma_{ij}^{-[1]} - \varepsilon_{ij}^{-[1]} \sigma_{ij}^{-[0]} \right] + O(\lambda^2) \right) \\ &\times \left(\delta \bar{v}_n^{[0]} + \lambda \delta \bar{v}_n^{[1]} + O(\lambda^2) \right) d\Gamma + \int_{\Gamma_{\text{gb}}^y} \gamma \left(\frac{\partial \left(\delta \bar{v}_s^{[0]} + \lambda \delta \bar{v}_s^{[1]} + O(\lambda^2) \right)}{\partial s} + \frac{\left(\delta \bar{v}_n^{[0]} + \lambda \delta \bar{v}_n^{[1]} + O(\lambda^2) \right)}{R} \right) d\Gamma \\ &+ \int_{\Gamma_{\text{gb}}^y} \frac{\left(\delta \bar{v}_n^{[0]} + \lambda \delta \bar{v}_n^{[1]} + O(\lambda^2) \right)}{\mu} \left(\bar{v}_n^{[0]} + \lambda \bar{v}_n^{[1]} + O(\lambda^2) \right) d\Gamma = 0. \end{aligned} \tag{4.35}$$

Note that in the above equation we have used the mapping relation $\int_{\Gamma_{\text{gb}}} (\cdot) d\Gamma = \lambda \int_{\Gamma_{\text{gb}}^y} (\cdot) d\Gamma$ in Eq. (3.13). The two leading order equations are:

$$\int_{\Omega^y} \frac{1}{2} \left[\varepsilon_{ij}^{+[0]} \sigma_{ij}^{+[0]} - \varepsilon_{ij}^{-[0]} \sigma_{ij}^{-[0]} \right] \delta \bar{v}_n^{[0]} d\Gamma + \int_{\Gamma_{\text{gb}}^y} \gamma \left(\frac{\partial \delta \bar{v}_s^{[0]}}{\partial s} + \frac{\delta \bar{v}_n^{[0]}}{R} \right) d\Gamma + \int_{\Gamma_{\text{gb}}^y} \frac{\delta \bar{v}_n^{[0]}}{\mu} \bar{v}_n^{[0]} d\Gamma = 0 \tag{4.36}$$

and

$$\int_{\Omega^y} \frac{1}{2} \left[\varepsilon_{ij}^{+[0]} \sigma_{ij}^{+[1]} + \varepsilon_{ij}^{+[1]} \sigma_{ij}^{+[0]} - \varepsilon_{ij}^{-[0]} \sigma_{ij}^{-[1]} - \varepsilon_{ij}^{-[1]} \sigma_{ij}^{-[0]} \right] \delta \bar{v}_n^{[1]} d\Gamma + \int_{\Gamma_{\text{gb}}^y} \frac{\delta \bar{v}_n^{[1]}}{\mu} \bar{v}_n^{[1]} d\Gamma = 0. \tag{4.37}$$

These two equations will be used to solve coarse and fine scale components of the grain boundary migration velocity. The multi-scale grain deformation and grain boundary migration equations discussed in Sections 4.1–4.4 are summarized in Box 1.

Box 1: Multi-scale grain deformation and grain boundary migration equations

1. Grain deformation velocity

- Coupling equation

$$v_k^{[1]} = \alpha_{kmn}(y) \hat{e}_{mn}^{[0]}(x),$$

$$\int_{\Omega^y} \beta_{imn,j} C_{ijkl} \eta_{klmn} \, d\Omega = - \int_{\Omega^y} \beta_{imn,j} C_{ijmn} \, d\Omega,$$

$$\eta_{ijmn} = \frac{1}{2} \left(\frac{\partial \alpha_{imn}}{\partial y_j} + \frac{\partial \alpha_{jmn}}{\partial y_i} \right).$$

- Coarse scale equation

$$\int_{\Omega^y} \frac{\partial w_i}{\partial x_j} \bar{C}_{ijkl} \hat{e}_{kl}^{[0]} \, d\Omega - \int_{\Gamma_h^y} w_i h_i \, d\Gamma - \int_{\Omega^y} w_i b_i \, d\Omega = 0,$$

$$\bar{C}_{ijmn} = \frac{1}{S} \int_{\Omega^y} C_{ijkl} (I_{klmn} + \eta_{klmn}) \, d\Omega.$$

2. Grain boundary velocity

- Coarse scale equation

$$\int_{\Omega^y} \frac{1}{2} \left[\varepsilon_{ij}^{+[0]} \sigma_{ij}^{+[0]} - \varepsilon_{ij}^{-[0]} \sigma_{ij}^{-[0]} \right] \delta \bar{v}_n^{[0]} \, d\Gamma + \int_{\Gamma_{gb}^y} \gamma \left(\frac{\partial \delta \bar{v}_s^{[0]}}{\partial s} + \frac{\delta \bar{v}_n^{[0]}}{R} \right) \, d\Gamma + \int_{\Gamma_{gb}^y} \frac{\delta \bar{v}_n^{[0]}}{\mu} \bar{v}_n^{[0]} \, d\Gamma = 0.$$

- Fine scale equation

$$\int_{\Omega^y} \frac{1}{2} \left[\varepsilon_{ij}^{+[0]} \sigma_{ij}^{+[1]} + \varepsilon_{ij}^{+[1]} \sigma_{ij}^{+[0]} - \varepsilon_{ij}^{-[0]} \sigma_{ij}^{-[1]} - \varepsilon_{ij}^{-[1]} \sigma_{ij}^{-[0]} \right] \delta \bar{v}_n^{[1]} \, d\Gamma + \int_{\Gamma_{gb}^y} \frac{\delta \bar{v}_n^{[1]}}{\mu} \bar{v}_n^{[1]} \, d\Gamma = 0.$$

5. Discretization and numerical procedures

A grain network as shown in Fig. 4 subjected to a surface traction is considered. Each grain is assumed to be orthotropic with orientations randomly assigned using a random number generator. Periodic boundary conditions are imposed on the boundary of the unit cell. As the grain boundary (GB) evolves, three topological changes are considered as shown in Fig. 5. The T1 and T2 changes were identified by Morral and Ashby [17]. A T1 change involves the switching of the grain boundaries when two triple points come very close to each other. T2 change represents the topological change of second kind where a three sided grain shrinks to a point. In numerical simulations, a T1 change might result in a two sided grain which again leads to topological instability in the grain network. This two sided grain is replaced by a single grain boundary and this topological transformation is called the third kind or a T3 change.

5.1. Approximation functions

In this approach, the coupling function α_{kmn} between the coarse and fine material velocities is solved based on the geometry of grain structure. If conventional finite element method is employed, a continuous

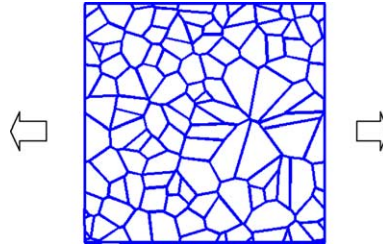


Fig. 4. Unit cell of a grain network subjected to horizontal constant traction.

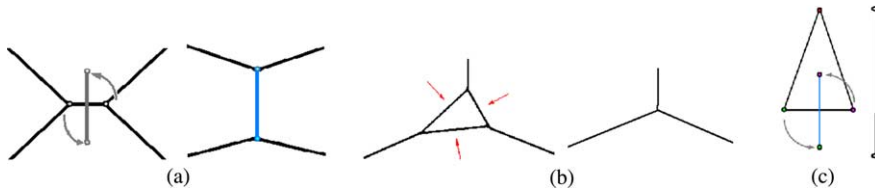


Fig. 5. Topological changes of grain boundaries: (a) T1 change; (b) T2 change; (c) T3 change.

remeshing is needed in the event of GB topological changes and the evolution of grain structures. Alternatively, the coupling function α_{kmn} can be approximated by meshfree shape functions constructed using moving least squares and reproducing kernel (MLS/RK) approximation [2,13] with grain boundary interface enrichment [28]. The GB velocity \bar{v} , on the other hand, is discretized by the finite element shape functions defined at the grain boundary points. Based on this discretization as shown in Fig. 6, we have

$$\alpha_{kmn}(\mathbf{y}) = \sum_{I=1}^{Nmp} \Psi_I(\mathbf{y}) \alpha_{kmnI}; \quad m, n, k = 1, 2, \quad (5.1)$$

$$\bar{v}_i^{[0]}(s) = \sum_{I=1}^{Ngbp} \bar{N}_I(s) \bar{v}_{iI}^{[0]}; \quad \bar{v}_i^{[1]}(s) = \sum_{I=1}^{Ngbp} \bar{N}_I(s) \bar{v}_{iI}^{[1]}, \quad (5.2)$$

where Nmp is the number of material points, $Ngbp$ is the number of grain boundary points, Ψ_I is the MLS/RK shape function, and $\bar{N}_I(s)$ is the one-dimensional finite element shape function defined along the grain boundary using grain boundary coordinate s shown in Fig. 7.

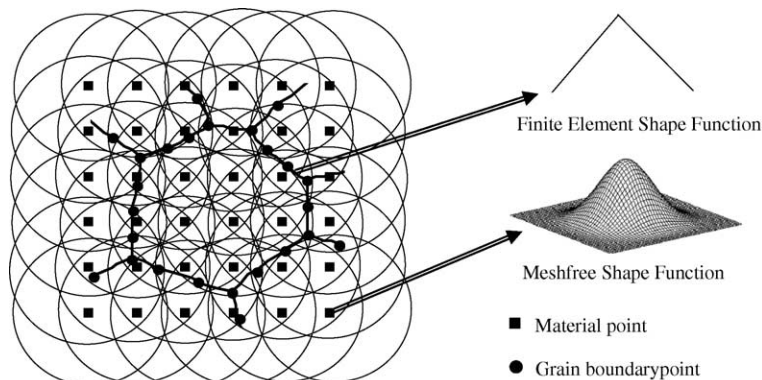


Fig. 6. Double-grid discretization of the fine scale variables.

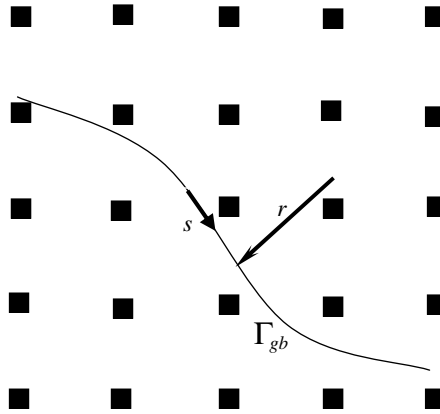


Fig. 7. Local coordinates of the discretized material interface.

Since the fine scale material velocity should exhibit a jump in its derivative in the normal direction along the grain boundary, the MLS/RK shape function Ψ_I for α_{kmn} is constructed following the grain boundary enriched reproducing kernel approximation [4,28] as

$$\Psi_I(\mathbf{y}) = \begin{cases} \hat{\psi}_I(\mathbf{y}), & \text{for nodes with } \mathbf{y}_I \in \Gamma_{gb} \\ \mathbf{H}^T(\mathbf{y} - \mathbf{y}_I)\mathbf{M}^{-1}(\mathbf{y})[\mathbf{H}(\mathbf{0}) - \sum_{I: \mathbf{x}_I \in \Gamma_{gb}} \hat{\psi}_I(\mathbf{y})\mathbf{H}(\mathbf{y} - \mathbf{y}_I)]\Phi_a(\mathbf{y} - \mathbf{y}_I), & \text{otherwise} \end{cases} \quad (5.3)$$

$$\mathbf{H}^T(\mathbf{y} - \mathbf{y}_I) = [1 \quad y_1 - y_{1I} \quad y_2 - y_{2I}], \quad (5.4)$$

$$\mathbf{M}(\mathbf{y}) = \sum_{I=1}^{N_{mp}} \mathbf{H}(\mathbf{y} - \mathbf{y}_I)\mathbf{H}^T(\mathbf{y} - \mathbf{y}_I)\Phi_a(\mathbf{y} - \mathbf{y}_I), \quad (5.5)$$

where Φ_a is the cubic B-spline function with support size “ a ”, and $\hat{\psi}_I$ is the interface enrichment function expressed as

$$\hat{\psi}_I(\mathbf{x}(r, s)) = \phi(r)\varphi(s). \quad (5.6)$$

The function $\phi(r)$ has a discontinuous derivative across the interface and $\varphi(s)$ is a smooth function along the interface. This interface enrichment function is defined locally on the interface with r and s being the local coordinates perpendicular to and along the interface, respectively, as shown in Fig. 7. The interface enrichment function $\hat{\psi}_I$ and its derivative are shown in Fig. 8. At the triple junction, the enrichment function $\phi(r)$ is constructed as

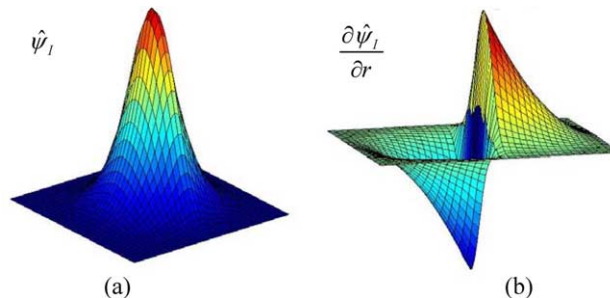


Fig. 8. (a) Interface enrichment function, (b) derivative of the interface enrichment function.

$$\phi(\mathbf{r}) = \phi(r_1) + \phi(r_2) + \phi(r_3) + \phi(r_1)\phi(r_2) + \phi(r_2)\phi(r_3) + \phi(r_1)\phi(r_3) + \phi(r_1)\phi(r_2)\phi(r_3), \quad (5.7)$$

where r_1, r_2, r_3 are the local coordinates of the three grain boundaries that form the triple junction.

5.2. Discrete equations

Using approximation functions for α_{kmn} in Eq. (5.1), the vector form of η_{klmn} in Eq. (4.18) can be expressed as

$$\boldsymbol{\eta} = \sum_{I=1}^r \mathbf{G}_I \boldsymbol{\alpha}_I, \quad (5.8)$$

where

$$\boldsymbol{\eta}^T = [\eta_{1111} \quad \eta_{1122} \quad \eta_{1112} \quad \eta_{2211} \quad \eta_{2222} \quad \eta_{2212} \quad 2\eta_{1211} \quad 2\eta_{1222} \quad 2\eta_{1212}], \quad (5.9)$$

$$\mathbf{G}_I = \begin{bmatrix} \Psi_{I,1} \mathbf{I} & \mathbf{0} \\ \mathbf{0} & \Psi_{I,2} \mathbf{I} \\ \Psi_{I,2} \mathbf{I} & \Psi_{I,1} \mathbf{I} \end{bmatrix}; \quad \Psi_{I,i} = \frac{\partial \Psi_I}{\partial y_i}, \quad (5.10)$$

$$\boldsymbol{\alpha}_I = \begin{bmatrix} \alpha_{1I} \\ \alpha_{2I} \end{bmatrix}; \quad \alpha_{1I} = \begin{bmatrix} \alpha_{111I} \\ \alpha_{122I} \\ \alpha_{112I} \end{bmatrix}; \quad \alpha_{2I} = \begin{bmatrix} \alpha_{211I} \\ \alpha_{222I} \\ \alpha_{212I} \end{bmatrix}. \quad (5.11)$$

Note that we have used the property $\alpha_{kmn} = \alpha_{knm}$. Here \mathbf{I} and $\mathbf{0}$ are 3×3 identity and zero matrices, respectively. Introducing the same approximation functions for the weight function β_{imn} , the discretization of the weak form equation (4.23) for solving the coupling function can be obtained as

$$\mathbf{P}\boldsymbol{\alpha} = \mathbf{q}, \quad (5.12)$$

where

$$\mathbf{P}_{IJ} = \int_{\Omega^v} \mathbf{G}_I^T \mathbf{C} \mathbf{G}_J \, d\Omega \quad (5.13)$$

and

$$\mathbf{q}_I = - \int_{\Omega^v} \mathbf{G}_I^T \boldsymbol{\Sigma} \, d\Omega, \quad (5.14)$$

$$\mathbf{C} = \begin{bmatrix} C_{1111} \mathbf{I} & C_{1122} \mathbf{I} & C_{1112} \mathbf{I} \\ C_{2211} \mathbf{I} & C_{2222} \mathbf{I} & C_{2212} \mathbf{I} \\ C_{1211} \mathbf{I} & C_{1222} \mathbf{I} & C_{1212} \mathbf{I} \end{bmatrix}, \quad (5.15)$$

$$\boldsymbol{\Sigma}^T = [C_{1111} \quad C_{1122} \quad C_{1112} \quad C_{2211} \quad C_{2222} \quad C_{2212} \quad C_{1211} \quad C_{1222} \quad C_{1212}]. \quad (5.16)$$

Due to the block structure of matrices, Eq. (5.12) can be solved using the following sub-matrices

$$\mathbf{p}\boldsymbol{\alpha}^{(i)} = \mathbf{q}^{(i)}; \quad i = 1, 3, \quad (5.17)$$

where

$$\mathbf{p}_{IJ} = \int_{\Omega^v} \mathbf{g}_I^T \mathbf{c}_J \, d\Omega, \quad (5.18)$$

$$\mathbf{q}_I^{(i)} = - \int_{\Omega^v} \mathbf{g}_I^T \boldsymbol{\Sigma}^{(i)} \, d\Omega, \quad (5.19)$$

$$\mathbf{g}_I = \begin{bmatrix} \Psi_{I,1} & 0 \\ 0 & \Psi_{I,2} \\ \Psi_{I,2} & \Psi_{I,1} \end{bmatrix}, \tag{5.20}$$

$$\mathbf{c} = \begin{bmatrix} C_{1111} & C_{1122} & C_{1112} \\ C_{2211} & C_{2222} & C_{2212} \\ C_{1211} & C_{1222} & C_{1212} \end{bmatrix}, \tag{5.21}$$

$$\boldsymbol{\alpha}_I^{(1)} = \begin{bmatrix} \alpha_{111I} \\ \alpha_{211I} \end{bmatrix}, \quad \boldsymbol{\alpha}_I^{(2)} = \begin{bmatrix} \alpha_{122I} \\ \alpha_{222I} \end{bmatrix}, \quad \boldsymbol{\alpha}_I^{(3)} = \begin{bmatrix} \alpha_{112I} \\ \alpha_{212I} \end{bmatrix}, \tag{5.22}$$

$$\boldsymbol{\Sigma}^{(1)} = \begin{bmatrix} C_{1111} \\ C_{2211} \\ C_{1211} \end{bmatrix}; \quad \boldsymbol{\Sigma}^{(2)} = \begin{bmatrix} C_{1122} \\ C_{2222} \\ C_{1222} \end{bmatrix}; \quad \boldsymbol{\Sigma}^{(3)} = \begin{bmatrix} C_{1112} \\ C_{2212} \\ C_{1212} \end{bmatrix}. \tag{5.23}$$

Upon obtaining the coupling function α_{kmn} , the homogenized material constitutive tensor \bar{C}_{ijkl} can be obtained by (4.32). The coarse scale material velocity $\mathbf{v}^{[0]}$ is then solved using the homogenized equation (4.33). First, let the approximation of $\mathbf{v}^{[0]}$ be expressed by

$$v_i^{[0]} = \sum_I N_I v_{iI}^{[0]}, \tag{5.24}$$

where N_I is the shape function. Introducing Eq. (5.24) and using the same shape functions for the weight function \mathbf{w} , the discrete homogenized equation (4.33) is obtained as

$$\mathbf{K}\mathbf{v}^{[0]} = \mathbf{f}, \tag{5.25}$$

where \mathbf{K} and \mathbf{f} are the standard stiffness matrix and force vector of elasticity. It is noted that the homogenized equation of the unit cell can be discretized with a very coarse mesh. Upon solving $\mathbf{v}^{[0]}$, the fine scale material velocity $\mathbf{v}^{[1]}$ is obtained using the coupling equation (4.16).

Using the coarse and fine scale material velocities $\mathbf{v}^{[0]}$ and $\mathbf{v}^{[1]}$, the strain rate $\dot{\boldsymbol{\varepsilon}}$, stress $\boldsymbol{\sigma}$, and strain energy density jump ($\boldsymbol{\varepsilon}^+ : \boldsymbol{\sigma}^+ - \boldsymbol{\varepsilon}^- : \boldsymbol{\sigma}^-$) that contribute to the grain boundary driving force in Eqs. (4.36) and (4.37) can be computed. By introducing approximation functions in Eq. (5.2) into grain boundary evolution (4.36) and (4.37), the coarse scale and fine scale grain boundary velocities $\bar{\mathbf{v}}^{[0]}$ and $\bar{\mathbf{v}}^{[1]}$ are solved from the following equations

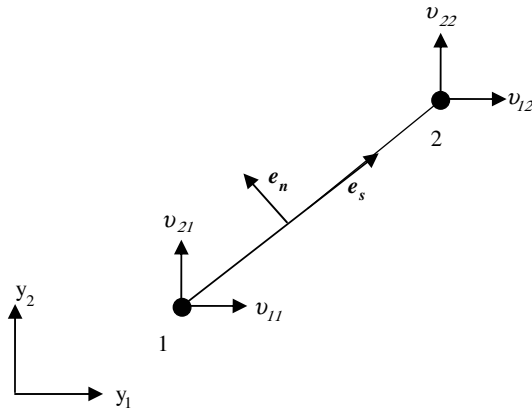


Fig. 9. Typical grain boundary element.

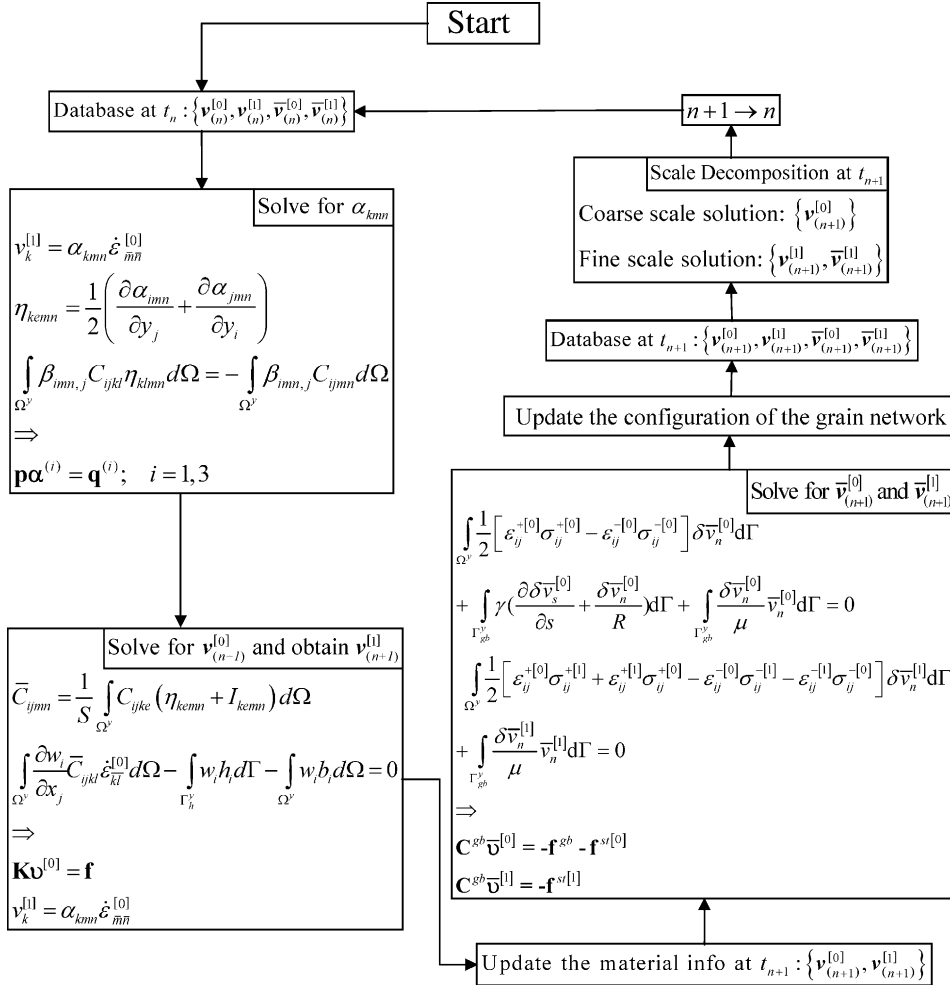


Fig. 10. Computational algorithm for multiple scale modeling of microstructure evolution.

$$\mathbf{C}_{\bar{v}}^{gb[0]} = -\mathbf{f}^{gb} - \mathbf{f}^{st[0]}, \tag{5.26}$$

$$\mathbf{C}_{\bar{v}}^{gb[1]} = -\mathbf{f}^{st[1]}, \tag{5.27}$$

where

$$\mathbf{C}_{IJ}^{gb} = \sum_{i=1}^{NGB} \int_{\Gamma_{gb(i)}^v} \frac{1}{\mu} \bar{\mathbf{N}}_I^T \mathbf{R}_n^T \mathbf{R}_n \bar{\mathbf{N}}_J ds, \tag{5.28}$$

$$\mathbf{f}_I^{gb} = \sum_{i=1}^{NGB} [\gamma_I \bar{\mathbf{N}}_I^T \mathbf{R}_n^T]_{s_i^2} + \sum_{i=1}^{NGB} \int_{\Gamma_{gb(i)}^v} \gamma \frac{\bar{\mathbf{N}}_I^T \mathbf{R}_n^T}{R} ds, \tag{5.29}$$

$$\mathbf{f}_I^{\text{st}[0]} = \sum_{i=1}^{\text{NGB}} \int_{\Gamma_{\text{gb}(i)}^y} \frac{1}{2} \left(\varepsilon_{ij}^{+[0]} \sigma_{ij}^{+[0]} - \varepsilon_{ij}^{-[0]} \sigma_{ij}^{-[0]} \right) \bar{\mathbf{N}}_I^T \mathbf{R}_n^T d\Gamma, \tag{5.30}$$

$$\mathbf{f}_I^{\text{st}[1]} = \sum_{i=1}^{\text{NGB}} \int_{\Gamma_{\text{gb}(i)}^y} \frac{1}{2} \left(\varepsilon_{ij}^{+[0]} \sigma_{ij}^{+[1]} + \varepsilon_{ij}^{+[1]} \sigma_{ij}^{+[0]} - \varepsilon_{ij}^{-[0]} \sigma_{ij}^{-[1]} - \varepsilon_{ij}^{-[1]} \sigma_{ij}^{-[0]} \right) \bar{\mathbf{N}}_I^T \mathbf{R}_n^T d\Gamma, \tag{5.31}$$

$$\bar{\mathbf{N}}_I = \begin{bmatrix} \bar{N}_I & 0 \\ 0 & \bar{N}_I \end{bmatrix}, \tag{5.32}$$

$$\mathbf{R}_n = [e_{nx} \quad e_{ny}], \tag{5.33}$$

$$\mathbf{R}_s = [e_{sx} \quad e_{sy}], \tag{5.34}$$

where the components of \mathbf{R}_n and \mathbf{R}_s are shown in Fig. 9, \bar{N}_I is the finite element shape function defined on the grain boundary, s_i^1 and s_i^2 are the two end points on the GB segment i , and NGB is the number of grain boundary segments. At each time step, the coupling function is obtained from (5.17), coarse scale and fine scale material velocities are obtained by Eqs. (5.25) and (4.16), respectively, and the grain boundary network under material deformation is updated. Eqs. (5.26) and (5.27) are then solved for the grain boundary migration velocity based on the deformed grain network, which again updates the grain network. The outline of the overall computational procedures is illustrated in Fig. 10.

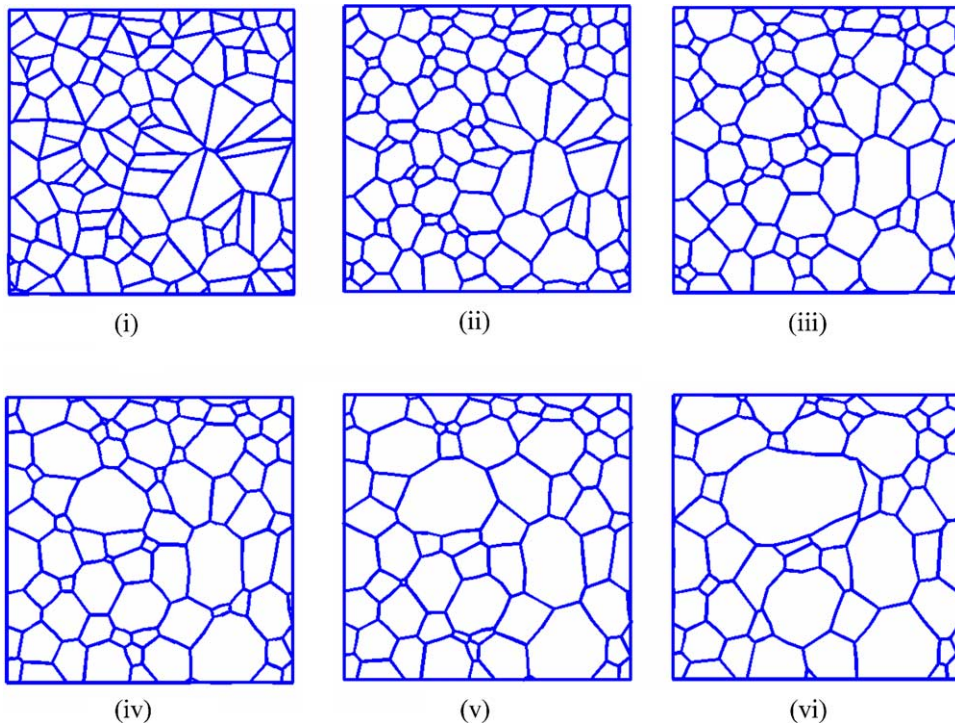


Fig. 11. Evolution of stressed grain growth.

6. Numerical example

In the numerical computation, the multi-scale evolution equations are solved in the referential domain. In this analysis, the following properties are used: unit cell box size = $1 \mu\text{m} \times 1 \mu\text{m}$, $\mu = 0.1 \mu\text{m}/\mu\text{N}/\text{s}$, $\gamma_b = 0.5 \mu\text{N}/\mu\text{m}$, orthotropic Young’s modulus $E_1 = 3 \times 10^5 \mu\text{N}/\mu\text{m}^2$, $E_2 = 2 \times 10^5 \mu\text{N}/\mu\text{m}^2$, the applied horizontal traction is $9.4 \times 10^6 \mu\text{N}/\mu\text{m}^2$, and time step size $\Delta t = 0.0004 \text{ s}$. Note that the grain deformation and grain boundary evolution equations are elliptic, and the time step size is determined by the minimum allowable grain boundary segment length when invoking topological changes for accuracy consideration. In each step, the coarse and fine scales of the grain material and grain boundary velocities are obtained, and the total deformation and grain boundary displacements are computed.

The grain structure evolution modeled by the proposed method is shown in Fig. 11. In agreement with the von Neumann relation [25] the grains with less than six edges continue to shrink and eventually disappear while those having more than six sides continue to grow. The components of the coupling function α_{ijk} at $t = 0.188 \text{ s}$ are plotted in Fig. 12. Since the coupling function relates coarse scale strain rate to the fine scale material velocity, the periodicity and the local character are shown in α_{ijk} distribution. Using α_{ijk} , the coarse scale material velocity is solved and the fine scale material velocity is thus obtained. The distribution of $v_i^{[0]}$ and $v_i^{[1]}$ are plotted in Fig. 13. Due to the constant traction in y_1 direction, the linear distribution of $v_1^{[0]}$ in y_1 direction, and linear distribution of $v_2^{[0]}$ in y_2 due to Poisson’s effect are correctly shown in Fig. 13. The distribution of $v_i^{[1]}$ in Fig. 13, on the other hand, demonstrates local fluctuation resulting from heterogeneity of grain structures. Coarse and fine scale strains for the last stage are also presented in Fig. 14.

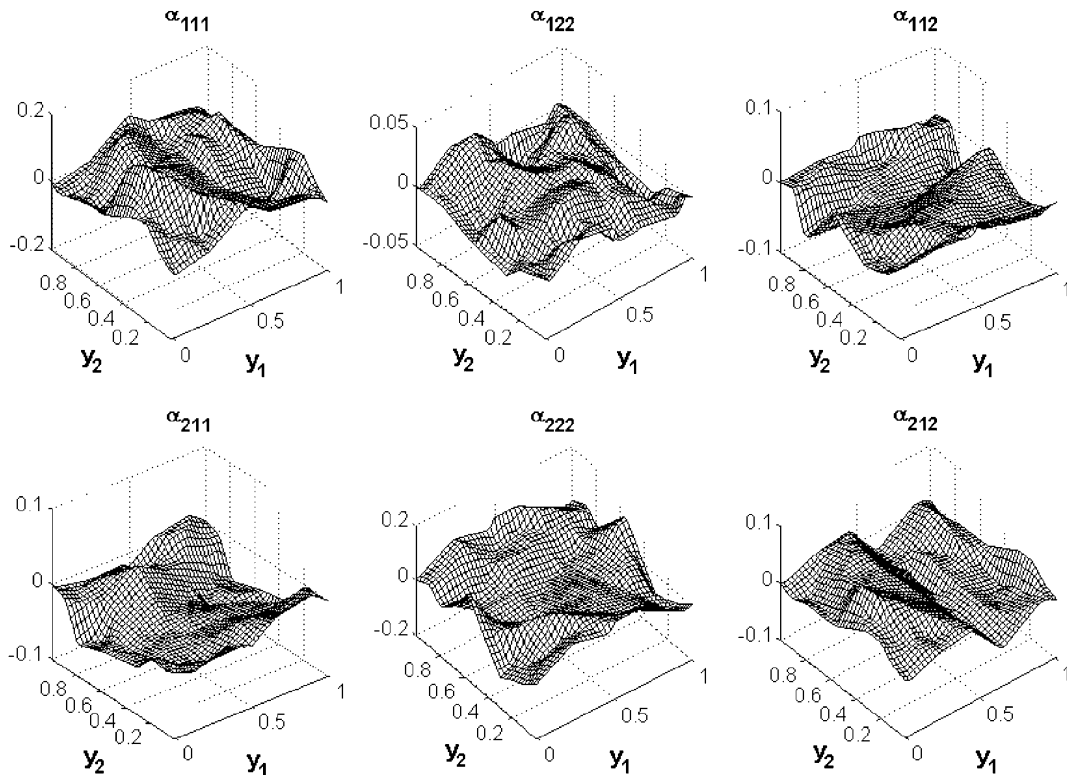


Fig. 12. Coupling functions at the final stage of grain evolution.

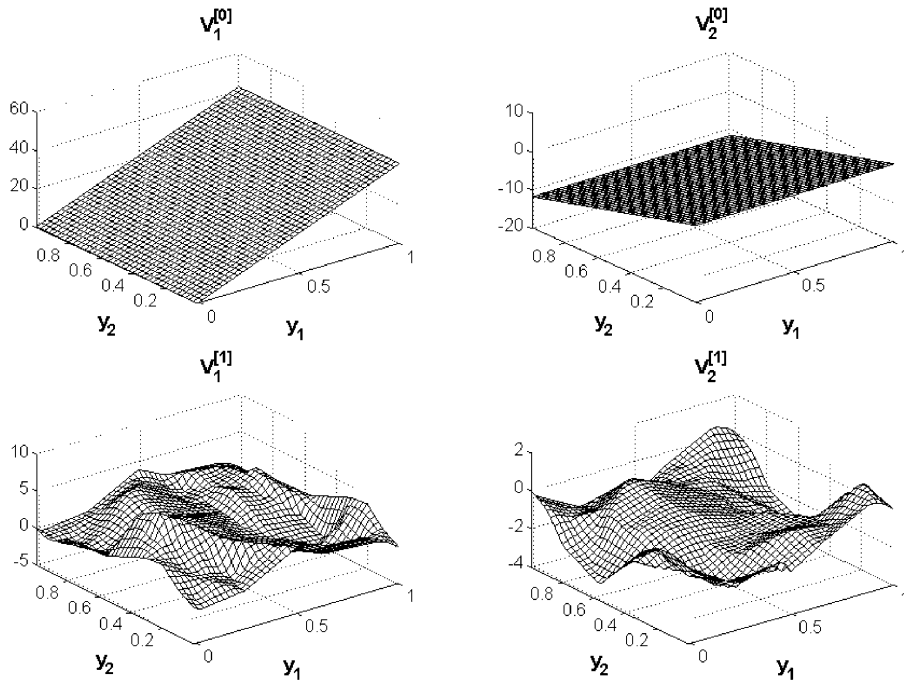


Fig. 13. Coarse and fine scale material velocities at the final stage of grain evolution.

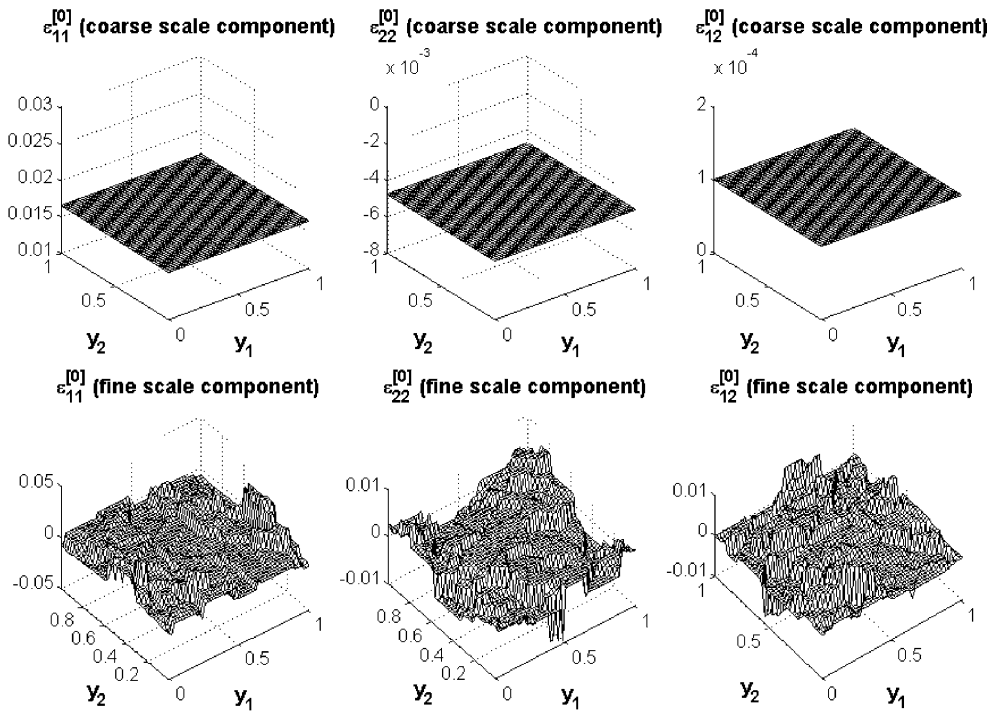


Fig. 14. Coarse and fine scale strains at the final stage of grain evolution.

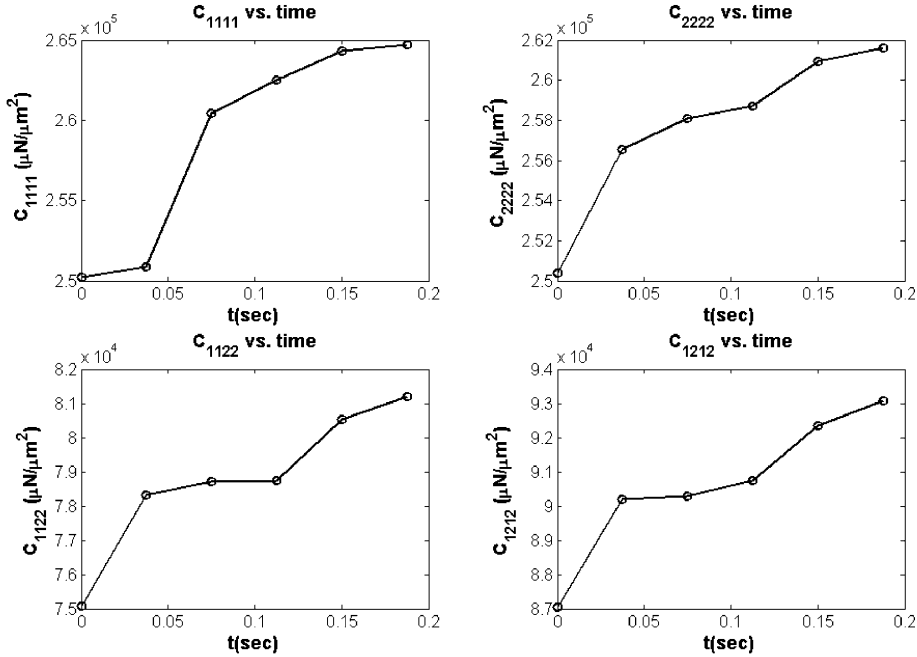


Fig. 15. Evolution of homogenized material properties during the grain structure evolution.

The homogenized \bar{C}_{1111} , \bar{C}_{2222} , \bar{C}_{1122} , and \bar{C}_{1212} components at a few selected states are shown in Fig. 15. It is interesting to observe that the material constants increase as the microstructures evolve. This phenomenon can be explained by two reasons: (a) for the grain system to reduce total free energy, the grains with smaller strain energy density are forced to grow, while the ones with larger strain energy density are forced to shrink; (b) the strain energy density in a grain under deformation is inversely proportional to the rigidity of the grain. Item (b) can be easily illustrated by considering an one-dimensional elastic rod with length ℓ and Young’s modulus E_1 in $0 \leq x \leq a$, E_2 in $a \leq x \leq \ell$. The strain energy density W in each part of the material is

$$(1) \quad W = \begin{cases} \frac{\sigma^2}{2E_1} & \text{for } 0 \leq x \leq a \\ \frac{\sigma^2}{2E_2} & \text{for } a \leq x \leq \ell \end{cases} \quad \text{if stress } \sigma \text{ is applied at the two ends,} \quad (6.1)$$

$$(2) \quad W = \begin{cases} cE_2/2 & \text{for } 0 \leq x \leq a \\ cE_1/2 & \text{for } a \leq x \leq \ell \end{cases} \quad \text{if strain } \varepsilon \text{ is applied at the two ends,} \quad (6.2)$$

where $c = \left(\frac{\ell\varepsilon}{aE_2 + (\ell - a)E_1}\right)^2 E_1 E_2$.

Thus in both cases the material with lower Young’s modulus has higher strain energy density when under deformation. Therefore in the case of grain growth, if other driving forces are less significant compared to the driving force induced by the strain energy density jump across the grain boundaries, the grains with higher Young’s modulus (stiffer grains) will tend to grow due to their lower strain energy densities in the grain interiors. This is demonstrated in a grain growth modeling as shown in Fig. 16, where a material imperfection is introduced to the network of uniform isotropic hexagonal grains so that the central grain has Young’s modulus higher than the others. When a horizontal uniform tensile traction is applied, the center grain continues to grow in order to minimize the total free energy. This explains why in the random

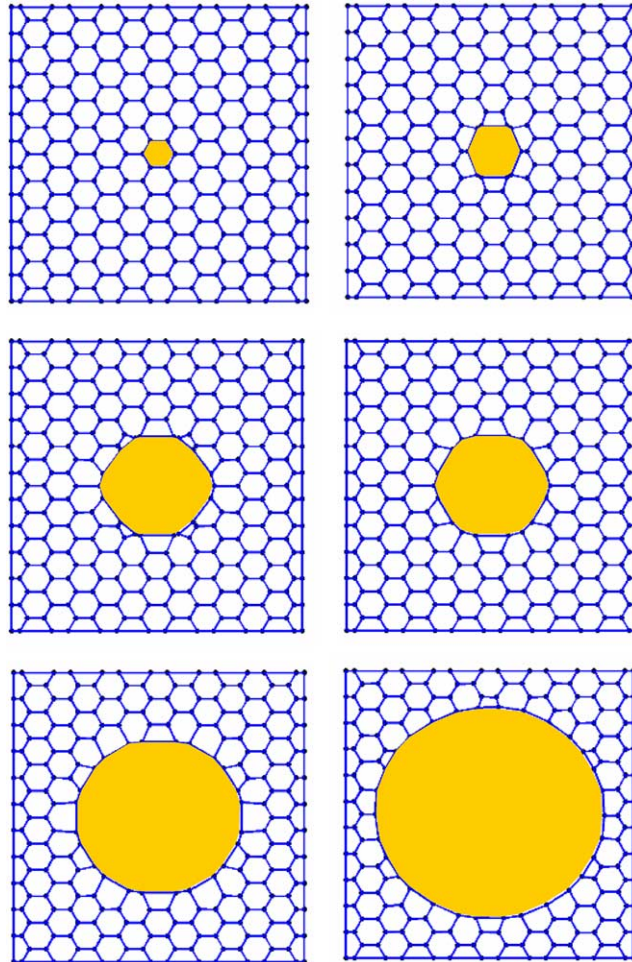


Fig. 16. Imperfection with a stiffer grain.

grain structure case as shown in Figs. 11–15, the homogenized material properties become stiffer as the grain structures evolve.

7. Conclusion

Understanding how the macroscopic external load affects the meso-scale grain growth process and how the grain structure influences the macro-scale property of the continuum represents an interesting multi-scale problem. The material velocity and grain boundary velocity are the two primary multi-scale variables involved in grain growth process; each plays different but complementary role in the evolution of grain growth. The material velocity represents the degree of grain deformation in response to the macroscopic external load. Due to the heterogeneity of the grain structure, the material velocity exhibits both coarse and fine scale characteristics. Consequently, the strain rate, stress, and strain energy density in each grain present multi-scale properties. The multi-scale behavior of the grain boundary velocity, on the other hand,

is dictated by the multi-scale driving force motivated by the multi-scale strain energy density jump across the grain boundaries.

An asymptotic framework has been proposed to provide a systematic approach for multi-scale modeling and homogenization of stressed grain growth. To yield variationally consistent multi-scale governing equations and scale-coupling relation of grain growth processes, a variational equation based on the principle of virtual power has been adopted as the basis of this work. By introducing the asymptotic form of the material velocity into the variational equation, the resulting leading order terms in the expanded variational equation yield multi-scale Euler equations representing grain structure equilibrium and grain boundary evolution equations. Using these multi-scale Euler equations, coupling function between coarse and fine material velocities was obtained, and Galerkin weak form was employed to solve the coupling function numerically. It was shown that due to the multi-scale property of the grain boundary driving force induced by the jumps in strain energy densities across the grain boundaries, the grain boundary velocity also takes a multi-scale form. With the scale-coupling function and multi-scale Euler equations, the homogenized elasticity tensor of the grain network unit cell has also been obtained.

In the numerical example demonstrated in this paper, the evolutions of coarse and fine scale grain kinematics and deformation have been presented. The evolution of homogenized material properties has also been obtained. It was shown that the overall stiffness of the grain network increases as the grain structure evolves. This is due to the nature for the grain system to reduce the total free energy to reach a stable configuration. As a consequence, stiffer grains which contain less strain energy density gain stronger driving force to grow if other driving forces are less significant compared to the driving force induced by the strain energy density jump across the grain boundaries.

Through the decomposition of kinematic and kinetic measures of grain deformation and grain boundary migration, one can filter out the gross response of the stressed grain network and extract the local fine scale information for investigation of several important grain boundary mechanisms such as grain boundary separation and diffusion processes. These studies will be the future extension of this work.

Acknowledgements

The support of this work by NSF under grant CMS 0084589 to University of California, Los Angeles is greatly acknowledged.

References

- [1] N.S. Bakhvalov, G.P. Panasenko, *Homogenization of Periodic Medium Process*, Nauka, Moscow, 1984.
- [2] T. Belytschko, Y.Y. Lu, L. Gu, Element-free Galerkin methods, *Int. J. Numer. Methods Engrg.* 37 (1994) 229–256.
- [3] A. Bensoussan, J.L. Lions, G. Papanicolau, *Asymptotic Analysis for Periodic Structures*, North Holland, Amsterdam, 1978.
- [4] J.S. Chen, V. Kotta, H. Lu, D. Wang, D. Moldovan, D. Wolf, Variational formulation and double-grid method for mesoscale modeling of stressed grain growth, *Comput. Methods Appl. Mech. Engrg.*, in press.
- [5] C.R. Chiang, The grain size effect on the flow stress of polycrystals, *Scripta Metall.* 19 (1985) 1281–1283.
- [6] J. Fish, K. Shek, Multi-scale analysis of composite materials and structures, *Compos. Sci. Technol.* 60 (12–13) (2000) 2547–2556.
- [7] J. Fish, V. Belsky, Multigrid method for periodic heterogeneous media. 1. Convergence studies for one-dimensional media, *Comput. Methods Appl. Mech. Engrg.* 126 (1–2) (1995) 1–16.
- [8] K. Garikipati, T.J.R. Hughes, A study of strain localization in a multiple scale framework—The one-dimensional problem, *Comput. Methods Appl. Mech. Engrg.* 159 (3–4) (1998) 193–222.
- [9] K. Garikipati, T.J.R. Hughes, A variational multi-scale approach to strain localization—formulation for multi-dimensional problems, *Comput. Methods Appl. Mech. Engrg.* 188 (1–3) (2000) 39–60.
- [10] Y. Han, M.C. Chaturvedi, J.R. Cahoon, Effect of grain size on the steady-state creep rate of inconel-718, *Scripta Metall.* 22 (1988) 255–260.

- [11] A.J. Haslam, D. Moldovan, S.R. Phillpot, D. Wolf, H. Gleiter, Combined atomistic and mesoscale simulation of grain growth in nanocrystalline thin films, *Comput. Mater. Sci.* 23 (2002) 15–32.
- [12] J. Knap, M. Ortiz, An analysis of the quasicontinuum method, *J. Mech. Phys. Solids* 49 (9) (2001) 1899–1923.
- [13] W.K. Liu, S. Jun, S. Li, J. Adee, T. Belytschko, Reproducing kernel particle methods for structural dynamics, *Int. J. Numer. Methods Engrg.* 38 (1995) 1655–1679.
- [14] W.K. Liu, W. Hao, Y. Chen, S. Jun, J. Gosz, Multiresolution reproducing kernel particle methods, *Comput. Mech.* 20 (4) (1997) 295–309.
- [15] W.K. Liu, Y. Chen, C.T. Chang, T. Belytschko, Advances in multiple scale kernel particle methods, *Comput. Mech.* 18 (2) (1996) 73–111.
- [16] W.K. Liu, E.G. Karpov, S. Zhang, H.S. Park, An introduction to computational nanomechanics and materials, *Comput. Methods Appl. Mech. Engrg.*, in press.
- [17] J.E. Morral, M.F. Ashby, Dislocated cellular structures, *Acta Metall.* 22 (1974) 567–575.
- [18] J.T. Oden, T.I. Zohdi, Analysis and adaptive modeling of highly heterogeneous elastic structures, *Comput. Methods Appl. Mech. Engrg.* 148 (1997) 367–391.
- [19] J.T. Oden, K. Vemaganti, N. Moes, Hierarchical modeling of heterogeneous solids, *Comput. Methods Appl. Mech. Engrg.* 172 (1999) 3–25.
- [20] E. Sanchez-Palencia, A. Zaoui, *Homogenization Techniques for Composites, Homogenization Techniques for Composite Media*, Springer-Verlag, Berlin, 1985.
- [21] O.A. Shenderova, D.W. Brenner, A.A. Nazarov, A.E. Romanov, L.H. Yang, Multi-scale modeling approach for calculating grain boundary energies from first principle, *Phys. Rev. B* 57 (6) (1998).
- [22] V.B. Shenoy, R. Miller, E.B. Tadmor, M. Ortiz, An adaptive finite element approach to atomic-scale mechanics—the quasicontinuum method, *J. Mech. Phys. Solids* 47 (3) (1999) 611–642.
- [23] E.B. Tadmor, M. Ortiz, R. Phillips, Quasicontinuum analysis of defects in solids, *Philos. Mag. A* 73 (6) (1996) 1529–1563.
- [24] V. Vaithyanathan, C. Wolverton, L.Q. Chen, Multi-scale modeling of precipitate microstructure evolution, *Phys. Rev. Lett.* 88 (12) (2002).
- [25] J. von Neumann, Discussion Remark Concerning Paper of C.S. Smith, *Grain Shapes and Other Metallurgical Applications of Topology*, American Society for Metals, Cleveland, OH, 1952, pp. 108–110.
- [26] G.J. Wagner, W.K. Liu, Hierarchical enrichment for bridging scales and meshfree boundary conditions, *Int. J. Numer. Methods Engrg.* 50 (2000) 507–524.
- [27] G.J. Wagner, W.K. Liu, Coupling of atomic and continuum simulations using a bridging scale decomposition, *J. Comput. Phys.* 190 (2003) 249–274.
- [28] D. Wang, J.S. Chen, Homogenization of magnetostrictive particle-filled elastomers using meshfree method with interface discontinuity, Invited for publication in special issue of *J. Finite Element Anal. Design* (Finalist of Robert Melosh student paper competition), in press.
- [29] Q. Yu, J. Fish, Multi-scale asymptotic homogenization for multi-physics problems with multiple spatial and temporal scales: a coupled thermo-viscoelastic example problem, *Int. J. Solids Struct.* 39 (2002) 6429–6452.
- [30] L. Zhang, W.K. Liu, S. Li, D. Qian, S. Hao, Survey of multi-scale meshfree particle methods, *Lecture Notes Comput. Sci. Engrg.* (2002) 441–458.